This is an open access article published under an ACS AuthorChoice License, which permits copying and redistribution of the article or any adaptations for non-commercial purposes.

ACS OMEGA

Article

Cite This: ACS Omega 2018, 3, 7639−7647

Pd NP-Decorated N-Rich Porous Organic Polymer as an Efficient Catalyst for Upgradation of Biofuels

Piyali Bhanja,[†] Kajari Ghosh,[‡] Sk Safikul Islam,[§,∥] Sk Manirul Islam,[§] and Asim Bhaumik*[,†]

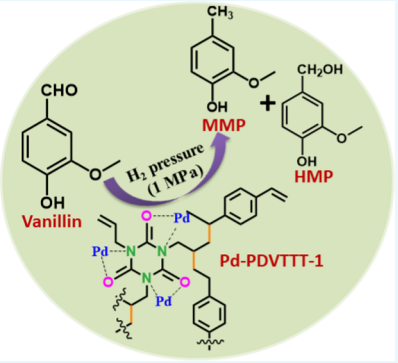
[†]Department of Materials Science, Indian Association for the Cultivation of Science, 2A and 2B Raja S. C. Mullick Road, Jadavpur 700032, West Bengal, India

[‡]Department of Chemistry, University of Burdwan, Golapbag Campus, Bardhaman 713104, West Bengal, India

[§]Department of Chemistry, University of Kalyani, Nadia 741235, West Bengal, India

Supporting Information

ABSTRACT: Hydrodeoxygenation process is a potential route for upgrading biofuel intermediates, like vanillin, which is obtained in huge quantities through the chemical treatment of the abundant lignocellulosic biomass resources of nature, and this is attracting increasing attentions over the years. Herein, we report the grafting of palladium nanoparticles at the surface of porous organic polymer Pd-PDVTTT-1 synthesized through the co-condensation of 1,3,5-triallyl-1,3,5-triazine-2,4,6-(1*H*,3*H*,5*H*)-trione and divinylbenzene in the presence of radical initiator under solvothermal reaction conditions. The Pd-PDVTTT-1 material has been characterized thoroughly by powder X-ray diffraction, nitrogen sorption, ultra-high-resolution transmission electron Microscopy, Fourier-transform infrared spectroscopy, ^{13}C MAS NMR, and X-ray photoelectron spectroscopy analyses. High surface area together with good thermal stability of the Pd-PDVTTT-1 material has motivated us to explore its potential as heterogeneous catalyst in the hydrodeoxygenation of vanillin for the production of upgraded biofuel 2-methoxy-4-methylphenol in almost quantitative yield and high selectivity (94%).



1. INTRODUCTION

Gradual decay of fossil fuel resources is a major concern of the 21st century for which the sustainable and innovative technologies for the conversion of renewable biomass into liquid fuels and chemicals are highly desirable.[1,2] Hydrodeoxygenation (HDO),[3,4] aqueous phase reforming,[5] and catalytic cracking[6] are the key chemical routes for the generation of biofuel from the abundant lignocellulosic biomass. Catalytic HDO reaction typically leads to byproducts with less amount of oxygen along with the introduction of greater thermal and chemical stability[7] of the products. Biofuel products obtained by using this catalytic HDO route can provide significant yields, and they offer lower CO_2 emissions upon combustion. Among all biosources, from wood-based biomass, the lignin content is over 30% and this is most abandoned in nature. Lignin can be depolymerized through chemical or biological cofermentation.[8] Various components of pyrolyzed oil that are obtained from lignin can be efficiently summed up for biofuel production. Thus, biofuel upgradation to liquid fuel for transportation by HDO is considered to be the most effective and feasible strategy compared with other methods like hydrogenolysis, decarbonylation, decarboxylation, and dehydration.[9] Vanillin (4-hydroxy-3-methoxybenzaldehyde) is one such component, having three different oxygenated functional groups (aldehyde, ether, and hydroxyl), and it is produced in huge quantities through the chemical treatment of these lignocellulosic biomass. Vanillin can be selectively hydrogenated into 2-methoxy-4-methylphenol (MMP), which is an indispensable future biofuel.[10] However, vanillin hydrogenation usually requires high pressure of hydrogen and high temperature, which always facilitates the formation of byproduct 4-hydroxymethyl-2-methoxyphenol (HMP) as a result of incomplete hydrogenation.

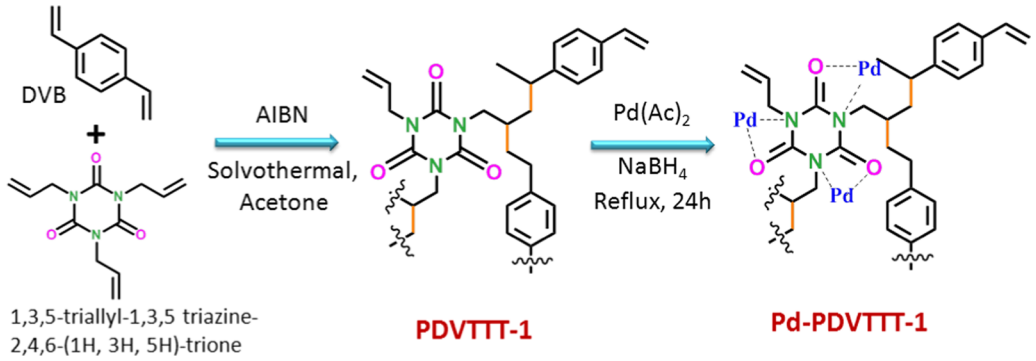
Today several strategies have been brought forward in designing the supported metal nanostructured materials as heterogeneous catalyst for this HDO reaction.[11] Platinum,[12] palladium,[13] ruthenium,[14,15] and rhodium[16]-based nanocatalysts showed high efficiency in upgrading vanillin via HDO. However, limited supply of these precious metal catalysts is always a major obstacle for these catalysts. This has motivated the researchers to develop the next generation heterogeneous catalysts for successful hydrodeoxygenation of vanillin. Nitrogen-containing high-surface-area porous nanomaterials found to be a very effective support, where palladium can be grafted at the pore surfaces for these organic transformations.[17−19] Owing to their tremendous potential in catalysis, a wide range of porous organic polymers (POPs)[20] including crystalline triazine-based frameworks,[21] conjugated microporous polymers,[22] microporous polymers,[23] polymers of intrinsic microporosity,[24] porous aromatic frameworks,[25] etc. are intensively

Received: May 3, 2018
Accepted: June 28, 2018
Published: July 10, 2018

 © 2018 American Chemical Society

DOI: 10.1021/acsomega.8b00892
ACS Omega 2018, 3, 7639−7647

Scheme 1. Schematic Representation for the Synthesis of Pd-PDVTTT-1 Porous Polymer



studied over the years. These POPs are largely synthesized through the polycondensation of a wide range of organic building blocks, and these materials possess large specific surface area, high thermal and mechanical stability, and good framework flexibility.[26] Furthermore, porous organic polymers bearing nitrogen-rich functionalities, like triazine, carbazole, amine, imine, and amide units, are efficiently utilized as heterogeneous catalysts for various organic transformations.[27,28] Because of high thermal and chemical stability, POPs can withstand the exposure of chemically unstable media and wet phase without disturbing their pore architecture.

Herein, we report the synthesis of a new N-rich porous organic polymer PDVTTT-1 through the co-polymerization of divinylbenzene and 1,3,5-triallyl-1,3,5-triazine-2,4,6-(1*H*,3*H*,5*H*)-trione monomers under solvothermal reaction conditions (Scheme 1). Since this nitrogen-rich polymeric framework exhibits high specific surface area, palladium NPs are grafted at the surface of the porous polymer through impregnation of Pd^0 from Pd(II) solution in the presence of a reducing agent. This Pd-grafted porous polymer has been utilized as a heterogeneous catalyst for hydrodeoxygenation of vanillin (a model system) for upgrading biofuels, which can be efficiently derived from lignin-based biomass.

2. RESULTS AND DISCUSSION

2.1. X-ray Diffraction Analysis. The wide-angle powder X-ray diffraction patterns of PDVTTT-1 and Pd-PDVTTT-1 are shown in Figure 1a,b, respectively. As seen from Figure 1a, the broad peak appeared at the 2θ value of 18−20°, which suggested the amorphous nature of the polymeric material. Powder X-ray diffraction pattern of Pd-PDVTTT-1 material, as shown in Figure 1b, displayed four peaks at 2θ values of 39.76, 46.31, 67.69, and 81.26°. These peaks could be assigned to the Pd(111), Pd(200), Pd(220), and Pd(311) face-centered cubic (fcc) crystal planes of metallic palladium nanoparticles.[29] Thus, this powder XRD data suggested successful loading of palladium nanoparticles at the surface of the porous organic polymer in PDVTTT-1.

2.2. Surface Area and Pore Size Measurement. To analyze the surface area and porosity of the POPs, nitrogen adsorption−desorption analysis has been carried out at 77 K. Figure 2a represents the nitrogen adsorption−desorption isotherms of PDVTTT-1, which can be classified as a mixture of type I and type IV with a very small hysteresis loop. The initial uptake of N_2 in the low pressure region (0.02−0.20 P/P_0) indicates the microporous nature of the material, and a very small hysteresis loop at the high pressure region (0.80−0.99 P/P_0) suggested the existence of interparticle porosity

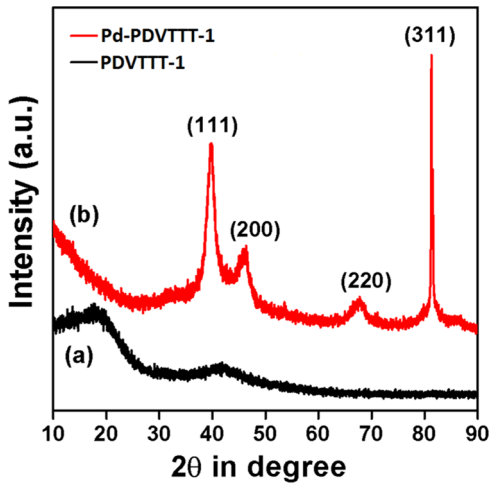


Figure 1. Wide-angle powder XRD pattern of PDVTTT-1 (a) and Pd-PDVTTT (b) samples.

throughout the polymeric matrix.[30] The nitrogen adsorption−desorption isotherms, as observed in Figure 2b, can be classified as typical type I, corresponding to the microporous nature of Pd-PDVTTT-1 material.[31] The Brunauer−Emmett−Teller (BET) surface area of these two materials PDVTTT-1 and Pd-PDVTTT-1 were 598 and 455 m^2/g, respectively. The estimated pore volumes of PDVTTT-1 and Pd-PDVTTT-1 samples were 0.3399 and 0.2201 $cm^3\ g^{-1}$, respectively. To measure the pore size distribution nonlocal density functional theory (NLDFT) method was employed. The pore size distributions for PDVTTT-1 and Pd-PDVTTT-1 materials have been estimated from their respective N_2 sorption isotherms' suggested peak pore size of 1.5 and 1.4 nm, respectively. This result suggested reduction of pore size and surface area after the grafting of Pd NPs at the POP surface.

2.3. Spectroscopic Analysis. To determine the various organic functionalities as well as chemical bonding in the polymeric framework, the Fourier-transform infrared (FTIR) spectroscopic analysis of the Pd-PDVTTT-1 has been carried out. Figure 3 represents the FTIR spectrum of Pd-PDVTTT-1 material, where the sharp signals at 2924 and 2848 cm^{-1} could be assigned to CH_2 and C−H stretching vibrations, respectively.[32] The characteristic peak at 1702 cm^{-1} could be assigned to the triazine ring containing carbonyl group. The peak at 1604 cm^{-1} is observed due to the presence of benzene moiety in the material framework. Further, two characteristic peaks appearing at 1374 and 1049 cm^{-1} are attributed to the existence of allyl-substituted triazine moiety in the polymeric

DOI: 10.1021/acsomega.8b00892
ACS Omega 2018, 3, 7639−7647

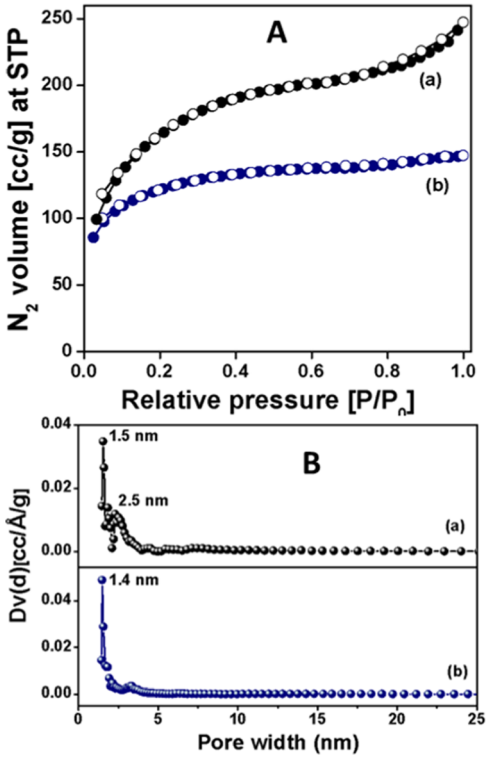


Figure 2. (A) Nitrogen adsorption−desorption isotherms of PDVTTT-1 (a) and Pd-PDVTTT-1 (b). (B) Respective pore size distribution plots of PDVTTT-1 (a) and Pd-PDVTTT-1 (b).

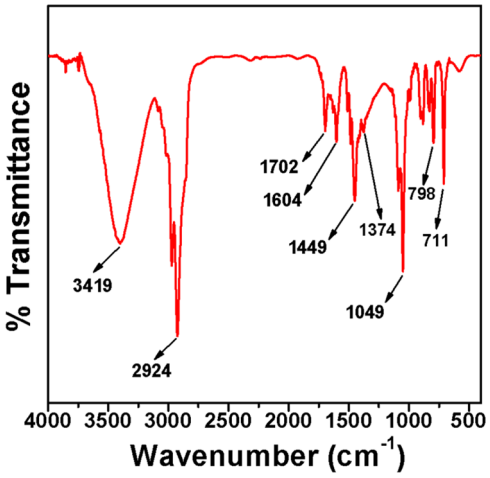


Figure 3. FTIR spectrum of Pd-PDVTTT-1 sample.

matrix.[33] The distinctive strong signal is noticed at 1449 cm^{-1} due to the aliphatic C−H bending vibration, and two other peaks appearing at 798 and 711 cm^{-1} are assigned to the presence of out-of-plane bending vibrations of aromatic C−H bond.

On the other hand, solid-state ^{13}C MAS NMR spectrum of the material has been recorded to understand about the chemical environment of different carbon centers in the porous polymer matrix. Figure 4 represents the solid-state ^{13}C MAS NMR spectrum of PDVTTT-1 polymer, where the triazine ring containing carbonyl carbon appeared at a chemical shift of 213.7 ppm and three characteristic signals at 152.7, 144.0, and 130.2 ppm are observed due to the presence of benzene ring containing carbons. The signal at 108.3 ppm indicated the

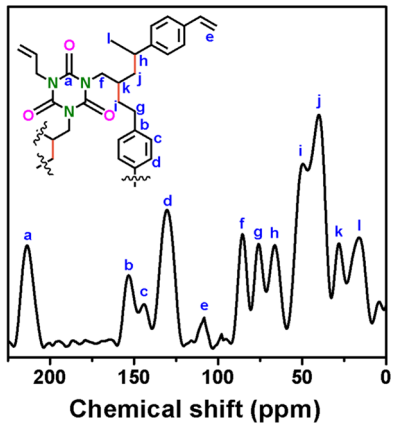


Figure 4. Solid-state ^{13}C CP MAS NMR spectrum of PDVTTT-1. Signals for different carbon atoms are marked in the inset model.

unreacted olefins in the material.[31] ^{13}C chemical shifts at 85.3, 75.6, 66.2, 49.6, 39.8, 28.2, and 15.7 ppm could be attributed to the different chemical environment of aliphatic carbon centers in PDVTTT-1. Thus, this ^{13}C CP MAS spectrum suggested the formation of porous polymer framework due to successful co-condensation of the monomers.

2.4. XPS Analysis. To evaluate the elemental composition as well as the oxidation state of supported Pd nanoparticles in the polymeric matrix, X-ray photoelectron spectroscopic analysis of Pd-PDVTTT-1 has been performed. Figure 5a,b represents the narrow-range XPS spectra of palladium, nitrogen, oxygen, and carbon atoms, whereas Figure 6 represents the full-range XPS spectrum of Pd-PDVTTT-1 material. The XPS spectrum of Pd exhibited two peaks with binding energy values of 335.0 and 340.1 eV, corresponding to Pd $3d_{5/2}$ and Pd $3d_{3/2}$, respectively. It is noticed that the binding energy values are slightly changed in comparison to those of Pd(0) state.[34] Thus, the high-resolution XPS spectrum of the Pd 3d matched well with that of Pd 3d of Pd(0), which is in good agreement with the existence of metallic Pd^0 species bound at the surface of the polymer framework. The amount of Pd loading in the polymer material has been estimated to be 2.28 wt % by employing CASA software. In Figure 6, full-range XPS spectrum of the material has been demonstrated, where N 1s, C 1s, and O 1s components are present with the binding energies of 399.1, 284.4, and 532.3 eV, respectively.

2.5. Microscopic Analysis. The high-resolution transmission electron microscopic image of the Pd-PDVTTT-1 material is shown in Figure 7. As seen from this figure, 2.0−3.0 nm size very small palladium nanoparticles are spread uniformly over the surface of the polymer material. Further, micropores having average pore diameter of 1.4 nm are seen throughout the specimen of Pd-PDVTTT-1 material. Thus, this electron microscopic result agrees well with the independent N_2 sorption analysis.

2.6. Thermal Stability. Thermogravimetric (TG) analysis has been carried out to determine the thermal stability of Pd-PDVTTT-1 material in the temperature range of 25−700 °C. Figure S1a (Supporting Information) represents the thermogravimetric analysis profile diagram, where the first weight loss starts from 290 to 395 °C due to the decomposition of organic functional group of the polymeric framework. The second weight loss up to 700 °C temperature could be attributed to the burning of the residual part of the material. So, the TG/DTA result suggested that the Pd-PDVTTT-1 material has

DOI: 10.1021/acsomega.8b00892
ACS Omega 2018, 3, 7639−7647

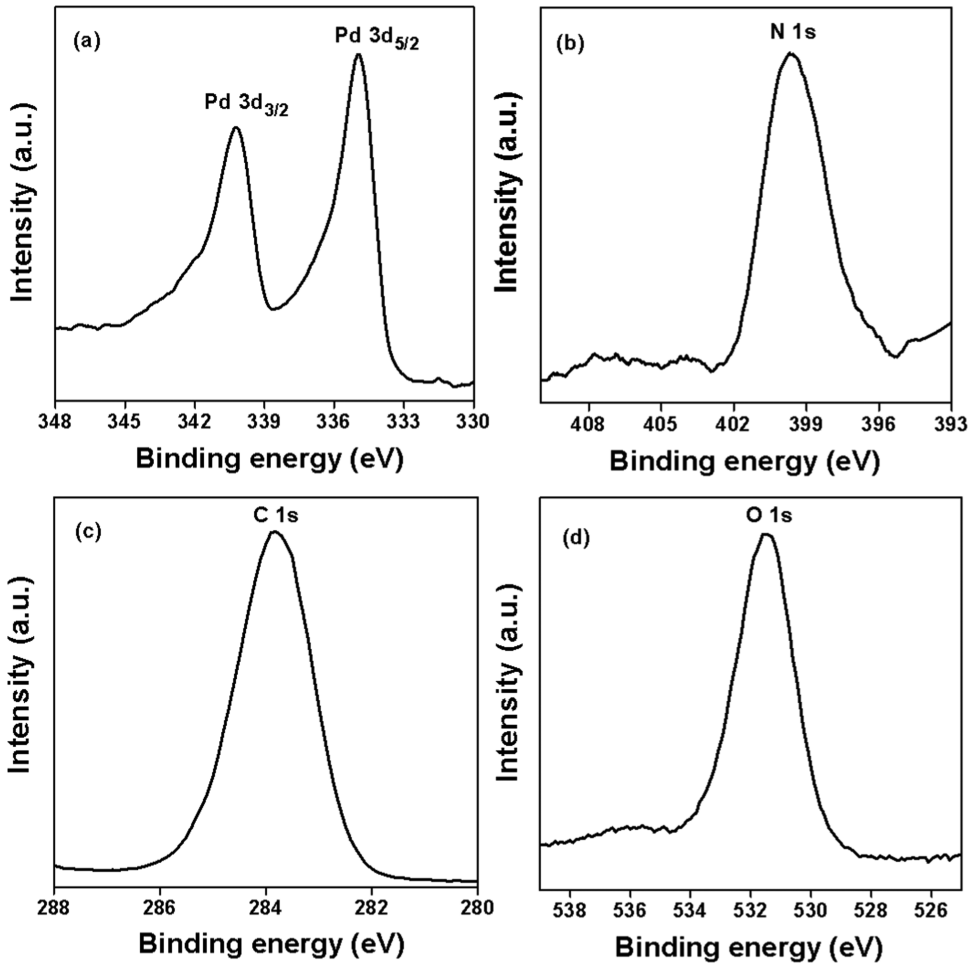


Figure 5. Narrow-range XPS spectra of Pd-PDVTTT-1 containing elements Pd 3d (a), N 1s (b), C 1s (c), and O 1s (d).

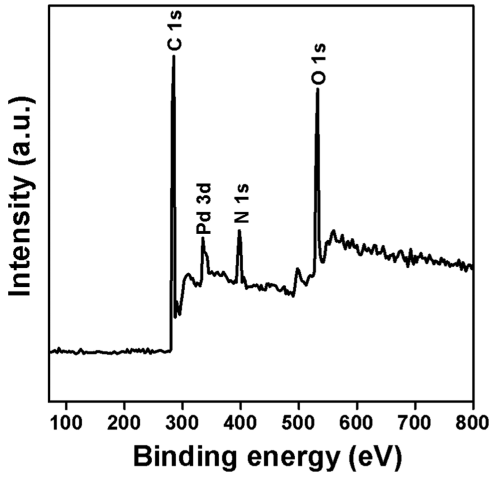


Figure 6. Full-range XPS spectrum of Pd-PDVTTT-1.

high thermal stability. The carbon, hydrogen, and nitrogen contents in the PDVTTT-1 polymeric framework were obtained experimentally, where C = 80.24%, H = 7.34%, and N = 6.83%. This elemental analysis result matches well with the theoretically calculations, where C = 81.00%, H = 7.14%, N = 5.45%, and O = 6.23%, as obtained from the stoichiometry of the framework of PDVTTT-1.

2.7. Basicity Measurement. Temperature-programmed desorption of CO_2 (CO_2-TPD) has been performed in the temperature range of 25−600 °C to measure the surface basic sites of the PDVTTT-1 polymer. The CO_2-TPD desorption profile of the sample was recorded by raising the temperature at a ramp of 5 °C/min using a thermal conductivity detector (TCD). As shown in Figure S2 (Supporting Information), two peaks are observed at 75 and 206 °C temperature in the TCD signal vs temperature profile diagram. These peaks could be assigned due to weak and strong basic sites, respectively, which can bind CO_2 molecules at the Pd-PDVTTT-1 surface. From the area under the desorption peak, the total strength of the basic sites has been estimated and this was 1.057 mmol g^{-1}.

2.8. Catalytic Activity. The catalytic efficiency of the Pd catalyst was investigated in the hydrodeoxygenation of vanillin. The schematic route for the hydrogenation of vanillin to MMP and HMP is shown in Scheme 2. At first, the reaction was carried out in Teflon-lined autoclave with 1 MPa H_2 pressure. The progress of the reaction was monitored by using gas chromatography (Varian GC-430) equipped with a flame ionization detector with a comparison of the chromatographic peak position with the known standards. After 5 h, when the gas chromatographic analysis was carried out with the filtrate, 36% conversion was noticed and HMP was found as the major product along with ∼8% MMP. After 12 h, GC analysis revealed the conversion has increased with the formation of MMP as the major product. Thus, it was concluded that with time, the selectivity of the product changes due to hydrogenolysis of vanillin alcohol. So, we decide to optimize the

DOI: 10.1021/acsomega.8b00892
ACS Omega 2018, 3, 7639−7647

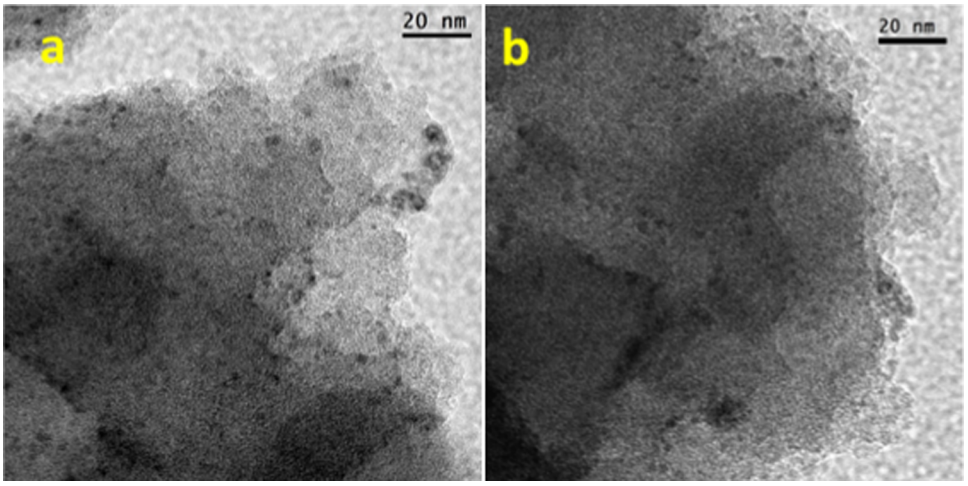
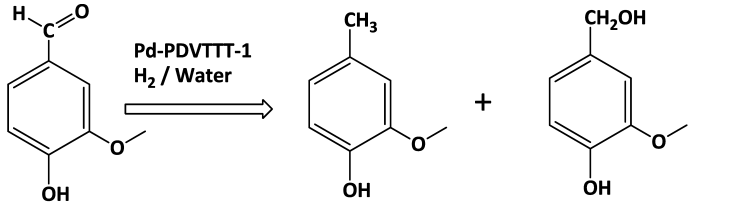


Figure 7. Ultra high resolution transmission electron microscopy images of Pd-PDVTTT-1 at different parts of the specimen (a, b).

Scheme 2. Hydrogenation of Vanillin to MMP and HMP over Pd-PDVTTT-1 Catalyst



reaction time, temperature, H_2 pressure, and amount of catalyst.

At first, the reaction was carried out without using catalyst. Even after 15 h, there was no conversion of vanillin. Then, the reaction was carried out with the support material only (35 mg of PDVTTT-1). In this case also, no conversion was observed. Thus, it can be concluded that the Pd NPs are necessary to carry out this HDO reaction. Then, we have carried out the reactions with different amounts of catalysts. Thirty-five milligrams of the supported Pd catalyst in the presence of other optimized reactants was best suited for the reaction because it resulted in the highest conversion of vanillin together with maximum selectivity of MMP. We have also tested some other supported catalysts, such as Pd-SBA-15 and commercially available Pd/C catalyst, to check the effect of support on the reaction. It has been observed that the non-nitrogenous supports are relatively less effective for this reaction compared with nitrogen-containing supports. In a suitable nitrogen-containing support, there is formation of electron-enriched Pd species in the catalyst, which is more active than Pd nanoparticles supported over N-free support materials.

The effect of H_2 pressure plays a key role in the hydrodeoxygenation of vanillin. The conversion was very poor at low H_2 pressure (<0.3 MPa). When the H_2 pressure was gradually increased to 0.5 MPa, the conversion of vanillin was also increased. At 0.8 MPa of H_2 pressure, 80% conversion of vanillin together with high selectivity for 2-methoxy-4-methylphenol (84%) was observed. Finally, at 1 MPa of H_2 pressure, 92% of conversion was observed for vanillin with 94% product selectivity for 2-methoxy-4-methylphenol (MMP). After optimization of the amount of catalyst and H_2 pressure needed for the reaction, we approached time optimization. Within 8 h, 48% of the vanillin was converted and vanillin alcohol (4-hydroxymethyl-2-methoxyphenol, HMP) was the major product (58%). The reaction was further carried out for further 6 h. The vanillin conversion was observed to be 88%. 2-Methoxy-4-methylphenol (MMP) was found as the major product with 84% selectivity. Selectivity of vanillin alcohol was thus decreased. As MMP is more valuable as biofuel than HMP, the reaction was further carried out for a longer time to get 2-methoxy-4-methylphenol with better selectivity. Finally, after 16 h, 97% of conversion was observed for vanillin with 94% product selectivity for MMP. Here, HMP was obtained as a byproduct (6% selectivity). The progress of the reaction was monitored by analyzing the reaction mixture through a GC. Generally, the hydrodeoxygenation of vanillin to 2-methoxy-4-methylphenol can proceed in two ways. First, vanillin can be hydrogenated to HMP, and then it is further hydrogenated to MMP. In another way, direct hydrogenolysis of the C═O may occur to give MMP. In our case, at first, hydrogenation of vanillin to HMP occurred and then the resulting HMP undergoes further hydrogenation and elimination of water to give MMP. At low temperatures (25−45 °C), very low conversion of vanillin was observed. High conversion of vanillin was observed on raising the temperature progressively beyond 80 °C. At 100 °C, more than 70% conversion was found. At 130 °C, a very good conversion of 85% was seen, and finally at 150 °C, an excellent conversion of 97% was observed together with 94% selectivity for MMP. Thus, 150 °C is the optimized reaction temperature for this HDO reaction over Pd-PDVTTT-1.

The effect of solvent on hydrodeoxygenation of vanillin was also examined under similar reaction conditions. Solvents like

DOI: 10.1021/acsomega.8b00892
ACS Omega 2018, 3, 7639−7647

tetrahydrofuran (THF), ethyl acetate, cyclohexane, and dimethyl formamide did not serve as appropriate solvents for this reaction and produced very poor to little conversion. When water was used as solvent for the hydrodeoxygenation of vanillin, quite good conversion was observed from the beginning. In 8 h time, nearly 48% conversion was observed, although at that time, the major product was vanillin alcohol. As satisfactory conversion could be obtained with water only, we continued the reaction for many hours to achieve better conversion of vanillin and also to get our target product 2-methoxy-4-methylphenol (MMP) in good yield with excellent selectivity. We have compared our catalyst with other Pd-supported catalysts, such as Pd/MSMF,[35] Pd/$CN_{0.132}$,[36] Pd/SO_3H-MIL-101,[37] and Pd@NH_2-UiO-66.[38] Our experimental results suggested that palladium nanoparticles are highly dispersed throughout the surface of this porous organic polymer. Here, Pd NPs are tightly bounded with the nitrogen atoms present in the framework of the porous polymer. Excess nitrogen sites in the material could help electron enrichment at the surface of Pd-PDVTTT-1. Electron-enriched supported palladium nanoparticles also showed high catalytic activity for the hydrogenation of vanillin.[39] Electron-enriched supported palladium nanoparticles could be responsible for high selectivity of MMP through the vanillin HDO process. N-rich material surfaces also improve the catalyst wettability in water. Thus, the contact of the substrates with the catalyst also increases, which ultimately gives better conversion. Further, Pd^0 impregnated on cubic mesoporous KIT-6 although showed 98% conversion of vanillin at 300 °C reaction in a vapor-phase down flow fixed-bed reactor for 6 h. But the reaction temperature is too high, and *p*-cresol is predominately formed in this upgradation process together with a small amount of vanillyl alcohol.[40] Thus, the nature of immobilized Pd^0 species together with the nature of the support plays a crucial role in the upgradation of vanillin to the value-added biofuel product MMP.

2.9. Reusability Test. For supported heterogeneous catalysts,[41−43] recycling efficiency is very crucial to ensure the chemical and thermal stability of the catalyst as well as for sustainable operation. We have reused the Pd-PDVTTT-1 catalyst for five consecutive cycles in HDO of vanillin. Initially, 35 mg of catalyst was employed for the HDO reaction under the optimized reaction condition and 97% conversion was achieved. Thereafter, the catalyst was removed by centrifugation and it was washed with methanol and dried in an oven at 80 °C for 6 h. This recovered catalyst was used for the next run under optimized reaction conditions. Similarly, we have performed total five catalytic cycles and corresponding product yields are shown in Figure 8. As seen from this figure, conversion of vanillin has been decreased by only 4.8% after five reaction cycles. This result suggested high recycling efficiency of Pd-PDVTTT-1 in the HDO of vanillin.

2.10. Leaching Test. To investigate the heterogeneity of the material, hot filtration test has been performed. The hydrodeoxygenation of vanillin (100 mg) was carried out in aqueous medium (15 mL) under H_2 pressure (1 MPa) inside the Teflon-lined reactor for 16 h at 150 °C temperature using 35 mg of the Pd catalyst. Then, the solution was filtered immediately during hot conditions to check if any Pd was being leached out from the solid support to the solution. Then, the same reaction was carried out using the filtrate for another 4 h. We could not observe any improvement of product yield before and after this hot filtration test. Thus, it can be concluded that Pd species could not be leached out from the porous polymer support and heterogeneity of Pd-PDVTTT-1 material has been retained.

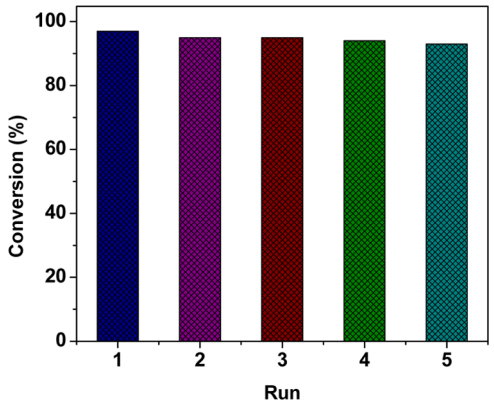


Figure 8. Recycling efficiency of Pd-PDVTTT-1 catalyst in the HDO of vanillin.

3. CONCLUSIONS

Palladium NPs are supported over nitrogen-rich porous organic polymer synthesized through the co-condensation of 1,3,5-triallyl-1,3,5-triazine-2,4,6-(1*H*,3*H*,5*H*)-trione and divinylbenzene under solvothermal reaction conditions. Both the parent porous polymer as well as its Pd-embedded analogue showed very high surface areas together with high chemical and mechanical stability. Because of the high loading of Pd^0 NPs at the surface of the porous organic polymer and their fine dispersion throughout the organic matrix, they act as an efficient heterogeneous catalyst for the selective hydrodeoxygenation of vanillin to upgraded biofuel product 2-methoxy-4-methylphenol. This study could encourage the researchers in developing supported Pd-catalysts based on N-rich porous polymers and exploring their catalytic activity for the biofuel upgradation via metal-mediated transfer hydrogenation process.

4. EXPERIMENTAL SECTION

4.1. Materials. Divinylbenzene (M_w = 130.19 g/mol) and 1,3,5-triallyl-1,3,5-triazine-2,4,6-(1*H*,3*H*,5*H*)-trione (M_w = 249.27 g/mol) were purchased from Sigma-Aldrich, India. Radical initiator azobisisobutyronitrile (AIBN; M_w = 164.21 g/mol) was obtained from SRL, India, and this was used after

Table 1. Effects of Catalysts on the Conversion and Selectivity of MMP in the HDO of Vanillin[a]

			selectivity (%)	
entry	catalyst amount (mg)	conversion (%)	MMP	HMP
1	no catalyst	0		
2	PDVTTT-1 (35)	0		
3	Pd-PDVTTT-1 (20)	55	64	36
4	Pd-PDVTTT-1 (30)	86	87	23
5	Pd-PDVTTT-1 (35)	97	94	6
6	Pd-PDVTTT-1 (40)	97	94	6
7	Pd/C (35)	64	67	33
8	Pd/SBA-15 (35)	82	42	58

[a]Reaction condition: vanillin (100 mg), water (15 mL), H_2 pressure (1 MPa), 150 °C, 16 h; 20−40 mg of the Pd catalyst, Pd loading in the catalyst Pd-PDVTTT-1 = 0.112 mmol/g.

DOI: 10.1021/acsomega.8b00892
ACS Omega 2018, 3, 7639−7647

Table 2. Effect of Reaction Temperature and Time of HDO of Vanillin over Pd-Pd-PDVTTT-1[a]

entry	reaction temperature (°C)	time (h)	conversion (%)
1	80	16	57
2	100	16	70
3	130	16	85
4	150	16	97
5	150	8	48
6	150	14	88
7	150	16	97
8	160	18	97

[a]Reaction condition: vanillin (100 mg), water (15 mL), H_2 pressure (1 MPa), 35 mg of the Pd-PDVTTT-1 catalyst, Pd loading in the catalyst = 0.112 mmol/g.

recrystallization. All organic solvents were obtained from Merck, India.

4.2. Synthesis of Porous Organic Polymer (PDVTTT-1). The porous organic polymer PDVTTT-1 was synthesized under solvothermal reaction conditions. In a typical synthesis, 0.004 mol divinylbenzene and 0.001 mol 1,3,5-triallyl-1,3,5-triazine-2,4,6-(1*H*,3*H*,5*H*)-trione were reacted through radical co-polymerization in the presence of azobisisobutyronitrile (AIBN) as a radical initiator. Initially, divinylbenzene was dissolved in 15 mL of dry acetone and then 1,3,5-triallyl-1,3,5-triazine-2,4,6-(1*H*,3*H*,5*H*)-trione was added to it and allowed to stir continuously for 30 min. To make inert atmosphere inside the whole system, nitrogen gas was purged continuously through the reaction mixture. Then, 25 mg of recrystallized AIBN was added to the solution mixture in one slot and the mixture was subjected to vigorous stirring for 1 h. Finally, the transparent slurry obtained in the process was loaded inside the Teflon-lined autoclave and kept for 24 h at 120 °C temperature. The solid product was collected by simple filtration technique and washed with acetone five times to get rid of unreacted starting monomers.

4.3. Synthesis of Pd-Grafted Porous Organic Polymer (Pd-PDVTTT-1). In the typical synthesis of Pd-grafted porous organic polymer Pd-PDVTTT-1, the as-synthesized polymer, 1.5 g of PDVTTT-1 was taken into the 100 mL round bottom flask containing 25 mL of absolute ethanol. Then, 0.3 g of palladium acetate was added to it, followed by slow adquadition of 0.3 g of sodium borohydride as a reducing agent and then the reaction mixture was refluxed for 24 h under nitrogen atmosphere. Finally, the gray solid sample was collected through filtration and washed using absolute ethanol. The dried solid product was subjected to thorough characterizations. The schematic representation for the formation of Pd-grafted porous organic polymer Pd-PDVTTT-1 is shown in Scheme 1.

4.4. General Procedure for the Catalytic Reactions. For the hydrodeoxygenation reaction, 100 mg of vanillin was taken in 15 mL of water and the mixture was placed under H_2 pressure (1 MPa) in a Teflon-lined reactor along with 35 mg of the Pd-PDVTTT-1 catalyst. This catalytic hydrodeoxygenation reaction was carried out at 150 °C for 16 h. The major product of the HDO of vanillin was 2-methoxy-4-methylphenol (MMP) together with a minor amount of byproduct 4-hydroxymethyl-2-methoxyphenol (HMP). The progress of the completion of the reaction was monitored by collecting aliquots and analyzing them by using capillary gas chromatography (Varian 6200 GC).

Table 3. Comparison of the Activity of Pd-PDVTTT-1 in the HDO of Vanillin with Related Catalytic Systems

entry	catalyst	reaction conditions	conv. (%)	sel. of MMP (%)	reference
1	Pd/MSMF	1 MPa in 20 mL of water containing 2 mmol vanillin at 110 °C for 2 h. Pd loading = 4.5 wt %	>99.5	>99.5	35
2	Pd/$CN_{0.132}$	150 °C, 1 MPa of H_2, water solvent, 6 h	100	100	36
3	Pd/SO_3H-MIL-101	vanillin, 2 mmol; water, 20 mL; amount of catalyst = 50 mg; hydrogen pressure, 0.5 MPa; reaction temperature, 80 °C	96.1	90.9	37
4	Pd@NH_2-UiO-66	vanillin, 2 mmol; water, 20 mL; amount of catalyst = 50 mg; hydrogen pressure, 0.5 MPa; reaction temperature, 90 °C	100	100	38
5	Pd-PDVTTT-1	vanillin (100 mg), water (15 mL), H_2 pressure (1 MPa), 150 °C, 16 h, 35 mg of the Pd catalyst, Pd loading 0.112 mmol/g	97.0	94.0	this work

DOI: 10.1021/acsomega.8b00892
ACS Omega 2018, 3, 7639−7647

4.5. Instrumentation. Powder X-ray diffraction patterns of the POP materials before and after Pd impregnations were recorded by using a Bruker D8 Advance SWAX diffractometer operated with 40 kV voltage and 40 mA current. The XRD instrument was calibrated by using a standard Si sample, and Ni-filtered Cu Kα radiation with wavelength λ of 0.154 06 nm used as the X-ray source. BET surface area and porosity of these materials were estimated from the respective N_2 sorption isotherms at 77 K by using a Quantachrome Instruments Autosorb-1C surface area analyzer. The samples were activated at 403 K under high vacuum for 12 h before the N_2 adsorption−desorption analysis. The pore size distributions were estimated from these N_2 sorption isotherms using the nonlocal density functional theory (NLDFT) and carbon/slit pore model as reference. For the high-resolution transmission electron microscopy analysis, a very small amount of the Pd-PDVTTT-1 sample was taken in absolute ethanol and finely dispersed in the medium through sonication for 5 min. Then, a small amount of the dispersed solution was dropped over a carbon-coated copper grid and this was dried under high vacuum before analysis. FTIR spectra of the samples were recorded on a PerkinElmer Spectrum 100 spectrophotometer, whereas solid-state ^{13}C CP MAS NMR spectrum was recorded by using a Bruker Advance 500 MHz NMR spectrometer. The thermogravimetric (TG) and differential thermal analysis (DTA) of Pd-PDVTTT-1 were recorded on TA-SDT Q-600 of TG instruments under air flow with a temperature ramp of 10 °C/min. The TPD analyzer TP-5080 of Micrometrics, was employed to obtain the temperature-programmed desorption of CO_2 (CO_2-TPD) on PDVTTT-1. After degassing the sample at 125 °C under inert atmosphere for 3 h, the sample was subjected for cooling down to room temperature, followed by 30 min purging with CO_2 gas in the U-shaped sample tube. Then, He gas was passed through the U-tube for 45 min to flush out any residual CO_2 gas present in the sample chamber. Then, the temperature of the system was increased and the respective CO_2-TPD profile was recorded. Further, for the determination of the chemical composition of PDVTTT-1, the carbon, hydrogen, and nitrogen contents in the material were recorded by using the Vario EL III CHNOS elemental analyzer (Tables 1−3).

■ ASSOCIATED CONTENT

Supporting Information

The Supporting Information is available free of charge on the ACS Publications website at DOI: 10.1021/acsomega.8b00892.

TG/DTA, CO_2-TPD profiles (PDF)

■ AUTHOR INFORMATION

Corresponding Author

*E-mail: msab@iacs.res.in.

ORCID

Asim Bhaumik: 0000-0002-4907-7418

Present Address

[||]Department of Chemistry, Aliah University, ll-A/27, Action Area II, Newtown, Action Area II, Kolkata 700156, West Bengal, India (S.S.I.).

Author Contributions

The manuscript was written through contributions of all authors. All authors have given approval to the final version of the manuscript.

Notes

The authors declare no competing financial interest.

■ ACKNOWLEDGMENTS

P.B. is grateful to CSIR, New Delhi for a junior research fellowship. A.B. wishes to acknowledge DST, New Delhi for the Indo-Egypt international project grant. K.G. acknowledges the Department of Science & Technology (DST) for her NPDF (PDF/2016/000160). S.M.I. acknowledges DST-SERB, UGC (New Delhi, Govt. of India) and DST-W.B. (West Bengal, India) for financial supports.

■ REFERENCES

(1) Huber, G. W.; Iborra, S.; Corma, A. Synthesis of Transportation Fuels from Biomass: Chemistry, Catalysts, and Engineering. *Chem. Rev.* **2006**, *106*, 4044−4098.

(2) Tilman, D.; Hill, J.; Lehman, C. Carbon-Negative Biofuels from Low-Input High-Diversity Grassland Biomass. *Science* **2006**, *314*, 1598−1600.

(3) Xue, Y.; Zhou, S.; Bai, X. L. Role of Hydrogen Transfer during Catalytic Copyrolysis of Lignin and Tetralin over HZSM-5 and HY Zeolite Catalysts. *ACS Sustainable Chem. Eng.* **2016**, *4*, 4237−4250.

(4) Lee, E. H.; Park, R.-S.; Kim, H.; Park, S. H.; Jung, S.-C.; Jeon, J.-K.; Kim, S. C.; Park, Y.-K. Hydrodeoxygenation of Guaiacol over Pt Loaded Zeolitic Materials. *J. Ind. Eng. Chem.* **2016**, *37*, 18−21.

(5) Vispute, T.; Huber, G. W. Production of Hydrogen, Alkanes and Polyols by Aqueous Phase Processing of Wood-Derived Pyrolysis Oils. *Green Chem.* **2009**, *11*, 1433−1445.

(6) Puértolas, B.; Keller, T. C.; Mitchell, S.; Pérez-Ramírez, J. Deoxygenation of Bio-Oil Over Solid Base Catalysts: From Model to Realistic Feeds. *Appl. Catal., B* **2016**, *184*, 77−86.

(7) Jiang, H.; Yu, X.; Peng, X.; Zhang, H.; Nie, R.; Lu, X.; Zhou, D.; Xia, Q. Efficient Aqueous Hydrodeoxygenation of Vanillin over a Mesoporous Carbon Nitride-Modified Pd Nanocatalyst. *RSC Adv.* **2016**, *6*, 69045−69051.

(8) He, Y. C.; Li, X. L.; Ben, H. X.; Xue, X. Y.; Yang, B. Lipid Production from Dilute Alkali Corn Stover Lignin by Rhodococcus Strains. *ACS Sustainable Chem. Eng.* **2017**, *5*, 2302−2311.

(9) De, S.; Saha, B.; Luque, R. Hydrodeoxygenation processes: Advances on Catalytic Transformations of Biomass-Derived Platform Chemicals into Hydrocarbon Fuels. *Bioresour. Technol.* **2015**, *178*, 108−118.

(10) Jiang, H. Z.; Yu, X. L.; Peng, X. L.; Zhang, H. F.; Nie, R. F.; Lu, X. H.; Zhou, D.; Xia, Q. H. Efficient Aqueous Hydrodeoxygenation of Vanillin Over A Mesoporous Carbon Nitride-Modified Pd Nanocatalyst. *RSC Adv.* **2016**, *6*, 69045−69051.

(11) Wang, H. L.; Ben, H. X.; Ruan, H.; Zhang, L. B.; Pu, Y. Q.; Feng, M. Q.; Ragauskas, A. J.; Yang, B. Effects of Lignin Structure on Hydrodeoxygenation Reactivity of Pine Wood Lignin to Valuable Chemicals. *ACS Sustainable Chem. Eng.* **2017**, *5*, 1824−1830.

(12) Ma, W.; Zhang, R.; Chen, G.; Liu, B. Hydrodeoxygenation of Vanillin over Various Metal Loading on ZSM-5/MCM-41 Under Mild Condition. *J. Biobased Mater. Bioenergy* **2017**, *11*, 308−312.

(13) Ibrahim, A. A.; Lin, A.; Zhang, F.; AbouZeid, K. M.; El-Shall, M. S. Palladium Nanoparticles Supported on a Metal-Organic Framework-Partially Reduced Graphene Oxide Hybrid for the Catalytic Hydrodeoxygenation of Vanillin as a Model for Biofuel Upgrade Reactions. *ChemCatChem* **2017**, *9*, 469−480.

(14) Yati, I.; Dwiatmoko, A. A.; Yoon, J. S.; Choi, J.-W.; Suh, D. J.; Jae, J.; Ha, J.-M. One-pot Catalytic Reaction to Produce High-Carbon-Number Dimeric Deoxygenated Hydrocarbons From Lignin-Derived Monophenyl Vanillin using Al_2O_3-Cogelled Ru Nanoparticles. *Appl. Catal., A* **2016**, *524*, 243−250.

DOI: 10.1021/acsomega.8b00892
ACS Omega 2018, 3, 7639−7647

(15) Yang, X.; Liang, Y.; Cheng, Y.; Song, W.; Wang, X.; Wang, Z.; Qiu, J. Hydrodeoxygenation of Vanillin over Carbon Nanotube-Supported Ru Catalysts Assembled at the Interfaces of Emulsion Droplets. *Catal. Commun.* **2014**, *47*, 28−31.
(16) Bengoechea, M. O.; Hertzberg, A.; Miletić, N.; Arias, P. L.; Barth, T. Simultaneous Catalytic De-Polymerization and Hydrodeoxygenation of Lignin In Water/Formic Acid Media with Rh/Al_2O_3, Ru/Al_2O_3 and Pd/Al_2O_3 as Bifunctional Catalysts. *J. Anal. Appl. Pyrolysis* **2015**, *113*, 713−722.
(17) Modak, A.; Mondal, J.; Sasidharan, M.; Bhaumik, A. Triazine Functionalized Ordered Mesoporous Polymer: a Novel Solid Support for Pd-Mediated C-C Cross-Coupling Reactions in Water. *Green Chem.* **2011**, *13*, 1317−1331.
(18) Singuru, R.; Dhanalaxmi, K.; Shit, S. C.; Reddy, B. M.; Mondal, J. Palladium Nanoparticles Encaged in a Nitrogen-Rich Porous Organic Polymer: Constructing a Promising Robust Nanoarchitecture for Catalytic Biofuel Upgrading. *ChemCatChem* **2017**, *9*, 2550−2564.
(19) Modak, A.; Pramanik, M.; Inagaki, S.; Bhaumik, A. A Triazine Functionalized Porous Organic Polymer: Excellent CO_2 Storage Material and Support for Designing Pd Nanocatalyst for C-C Cross-Coupling Reactions. *J. Mater. Chem. A* **2014**, *2*, 11642−11650.
(20) Modak, A.; Mondal, J.; Bhaumik, A. Porphyrin based porous organic polymer as bi-functional catalyst for selective oxidation and Knoevenagel condensation reactions. *Appl. Catal., A* **2013**, *459*, 41−51.
(21) Hug, S.; Mesch, M. B.; Oh, H.; Popp, N.; Hirscher, M.; Senker, J.; Lotsch, B. V. A Fluorene Based Covalent Triazine Framework with High CO_2 and H_2 Capture and Storage Capacities. *J. Mater. Chem. A* **2014**, *2*, 5928−5936.
(22) Xu, Y.; Mao, N.; Zhang, C.; Wang, X.; Zeng, J.; Chen, Y.; Wang, F.; Jiang, J.-X. Rational Design of Donor-π-Acceptor Conjugated Microporous Polymers for Photocatalytic Hydrogen Production. *Appl. Catal., B* **2018**, *228*, 1−9.
(23) Dübner, M.; Naoum, M.-E.; Spencer, N. D.; Padeste, C. From pH- to Light-Response: Post polymerization Modification of Polymer Brushes Grafted onto Microporous Polymeric Membranes. *ACS Omega* **2017**, *2*, 455−461.
(24) Elmehalmey, W. A.; Azzam, R. A.; Hassan, Y. S.; Alkordi, M. H.; Madkour, T. M. Imide-Based Polymers of Intrinsic Microporosity: Probing the Microstructure in Relation to CO_2 Sorption Characteristics. *ACS Omega* **2018**, *3*, 2757−2764.
(25) Vilian, A. T. E.; Puthiaraj, P.; Kwak, C. H.; Hwang, S.-K.; Huh, Y. S.; Ahn, W.-S.; Han, Y.-K. Fabrication of Palladium Nanoparticles on Porous Aromatic Frameworks as a Sensing Platform to Detect Vanillin. *ACS Appl. Mater. Interfaces* **2016**, *8*, 12740−12747.
(26) Alcaraz-Espinoza, J. J.; De Melo, C. P.; De Oliveira, H. P. Fabrication of Highly Flexible Hierarchical Polypyrrole/Carbon Nanotube on Eggshell Membranes for Supercapacitors. *ACS Omega* **2017**, *2*, 2866−2877.
(27) Zhang, Y.; Riduan, S. N. Functional Porous Organic Polymers for Heterogeneous Catalysis. *Chem. Soc. Rev.* **2012**, *41*, 2083−2094.
(28) Modak, A.; Mondal, J.; Aswal, V. K.; Bhaumik, A. A new periodic mesoporous organosilica containing diimine-phloroglucinol, Pd(II)-grafting and its excellent catalytic activity and trans-selectivity in C-C coupling reactions. *J. Mater. Chem.* **2010**, *20*, 8099−8106.
(29) Molla, R. A.; Bhanja, P.; Ghosh, K.; Islam, S. S.; Bhaumik, A.; Islam, S. M. Pd Nanoparticles Decorated on Hypercrosslinked Microporous Polymer: A Highly Efficient Catalyst for the Formylation of Amines through Carbon Dioxide Fixation. *ChemCatChem* **2017**, *9*, 1939−1946.
(30) Bhanja, P.; Chatterjee, S.; Bhaumik, A. Triazine-Based Porous Organic Polymer with Good CO_2 Gas Adsorption Properties and an Efficient Organocatalyst for the One-Pot Multicomponent Condensation Reaction. *ChemCatChem* **2016**, *8*, 3089−3098.
(31) Bhanja, P.; Gomes, R.; Bhaumik, A. N-rich Porous Organic Polymer With Suitable Donor-Donor-Acceptor Functionality for the Sensing of Nucleic Acid Bases and CO_2 Storage Application. *RSC Adv.* **2015**, *5*, 74916−74923.
(32) Yang, X.; Liang, Y.; Zhao, X.; Song, Y.; Hu, L.; Wang, X.; Wang, Z.; Qiu, J. Au/CNTs Catalyst for Highly Selective Hydrodeoxygenation of Vanillin at the Water/Oil Interface. *RSC Adv.* **2014**, *4*, 31932−31936.
(33) Tao, L.; Niu, F.; Zhang, D.; Wanga, T.; Wang, Q. Amorphous Covalent Triazine Frameworks for High Performance Room Temperature Ammonia Gas Sensing. *New J. Chem.* **2014**, *38*, 2774−2777.
(34) Yang, S.; Dong, J.; Yao, Z.; Shen, C.; Shi, X.; Tian, Y.; Lin, S.; Zhang, X. One-Pot Synthesis of Graphene-Supported Monodisperse Pd Nanoparticles as Catalyst for Formic Acid Electro-oxidation. *Sci. Rep.* **2014**, *4*, No. 4501.
(35) Lv, Z.; Sun, Q.; Meng, X.; Xiao, F.-S. Superhydrophilic Mesoporous Sulfonated Melamine-Formaldehyde Resin Supported Palladium Nanoparticles as an Efficient Catalyst for Biofuel Upgrade. *J. Mater. Chem. A* **2013**, *1*, 8630−8635.
(36) Xu, X.; Li, Y.; Gong, Y.; Zhang, P.; Li, H.; Wang, Y. Synthesis of Palladium Nanoparticles Supported on Mesoporous N-Doped Carbon and Their Catalytic Ability for Biofuel Upgrade. *J. Am. Chem. Soc.* **2012**, *134*, 16987−16990.
(37) Zhang, F.; Jin, Y.; Fu, Y.; Zhong, Y.; Zhu, W.; Ibrahim, A. A.; El-Shall, M. S. Palladium Nanoparticles Incorporated Within Sulfonic Acid-Functionalized MIL-101(Cr) for Efficient Catalytic Conversion of Vanillin. *J. Mater. Chem. A* **2015**, *3*, 17008−17015.
(38) Zhang, F.; Zheng, S.; Xiao, Q.; Zhong, Y.; Zhu, W.; Lin, A.; El-Shal, M. S. Synergetic Catalysis of Palladium Nanoparticles Encaged within Amine-Functionalized UIO-66 in the Hydrodeoxygenation of Vanillin in Water. *Green Chem.* **2016**, *18*, 2900−2908.
(39) Tedsree, K.; Tong, L.; Simon, J.; Chun, W. A. C.; Yu, K. M. K.; Bagot, P. A. J.; Marquis, E. A.; Smith, G. D. W.; Tsang, S. C. E. Hydrogen Production from Formic Acid Decomposition at Room Temperature using a Ag-Pd Core-Shell Nanocatalyst. *Nat. Nanotechnol.* **2011**, *6*, 302−307.
(40) Kayalvizhi, J.; Pandurangan, A. Hydrodeoxygenation of vanillin using palladium on mesoporous KIT-6 in vapour phase reactor. *Mol. Catal.* **2017**, *436*, 67−77.
(41) Liu, S.; Simonetti, T.; Zheng, W.; Saha, B. Selective Hydrodeoxygenation of Vegetable Oils and Waste Cooking Oils to Green Diesel Using a Silica-Supported Ir-ReOx Bimetallic Catalyst. *ChemSusChem* **2018**, *11*, 1446−1454.
(42) Liu, S.; Dutta, S.; Zheng, W.; Gould, N. S.; Cheng, Z.; Xu, B.; Saha, B.; Vlachos, D. G. Catalytic Hydrodeoxygenation of High Carbon Furylmethanes to Renewable Jet-fuel Ranged Alkanes over a Rhenium-Modified Iridium Catalyst. *ChemSusChem* **2017**, *10*, 3225−3234.
(43) Dutta, S.; Saha, B. Hydrodeoxygenation of Furylmethane Oxygenates to Jet and Diesel Range Fuels: Probing the Reaction Network with Supported Palladium Catalyst and Hafnium Triflate Promoter. *ACS Catal.* **2017**, *7*, 5491−5499.

DOI: 10.1021/acsomega.8b00892
ACS Omega 2018, 3, 7639−7647